Earth Planet. Sci. Lett. 681 (2026) 119920

Contents lists available at ScienceDirect

Earth and Planetary Science Letters

journal homepage: www.elsevier.com/locate/epsl

Subduction collapse and the isolation of southwest Gondwana basins from the Panthalassa Ocean

Guido M. Gianni [a,b,*], Federico Dávila [c,d], Cesar R. Navarrete [c], Gustavo Correa [c], Osvaldo Conde [c], Pietro Sternai [e]

[a] Institute of Geophysics of the Czech Academy of Sciences, Prague 1401, Czechia
[b] GFZ Helmholtz Centre for Geosciences, 14473 Potsdam Germany
[c] National Scientific and Technical Research Council (CONICET), Capital Federal 1414, Argentina
[d] Facultad de Ciencias Exactas, Físicas y Naturales, Universidad Nacional de Córdoba, Argentina
[e] Department of Earth and Environmental Sciences, University of Milano-Bicocca, Italy

ARTICLE INFO

Editor: Dr A Webb

Keywords:
Subduction interruption
Dynamic uplift
Orogenic collapse
Paleogeography
Panthalassa ocean

ABSTRACT

Late Paleozoic seaways in southwestern Gondwana intermittently connected the Panthalassa Ocean with the continental interior, shaping sedimentation, climate, and biogeography across forearc to intraplate basins. While the closure of southern marine inlets feeding intraplate regions is well explained by crustal thickening during the Gondwanide orogeny, the latest Permian–Early Triassic disconnection of western seaways supplying forearc and back-arc basins along the proto-Andean active margin remains enigmatic. This disconnection coincided with global deglaciation and with mid-Permian extensional collapse following proto-Andean mountain building (San Rafael orogeny), which is paradoxical. Here we test whether a large-scale interruption of subduction associated with the Choiyoi magmatic province could have generated margin-wide uplift sufficient to disrupt marine connections at this time. First-order dynamic topography models indicate that shutdown of subduction between ~275 and 250 Ma would have reversed dynamic subsidence and produced broad surface uplift of the Choiyoi magmatic belt. We propose that this uplift severed marine connections between the Panthalassa Ocean and western basins, forming an orographic barrier that, together with global climatic trends, promoted aridification across the continental interior.

1. Introduction

Seaway shifts, from ingressions to regressions, shape the climate by altering circulation and the transport of heat and moisture (Cane and Molnar, 2001). By acting as corridors or barriers, these shifts also control biotic dispersal, isolation, and extinction. In southwestern Gondwana, Late Paleozoic seaways periodically connected the Panthalassa Ocean with the supercontinent interior (Limarino and Spalletti, 2006) (Fig. 1a, b). These inlets enabled marine ingressions that linked multiple intraarc and backarc depocenters along the plate margin, while in the intraplate area, they were most prominently expressed in Permian times as the extensive Irati (Brazil)-Whitehill (South Africa) epicontinental sea, also known as the Mesosaurus Sea (Bastos et al., 2021; Limarino et al., 2014). These marine connections were progressively obstructed by the development of the Gondwanide orogen (Keidel, 1925). This Late Paleozoic fold-and-thrust belt extended along the western South American margin (San Rafaelic Orogen), across the North Patagonian Massif and the Sierras de la Ventana in Argentina, and into its South African counterpart, the Cape Fold Belt (Ramos et al., 2020) (Fig. 1b). Since pioneering studies, this mountain belt was conceived as a topographic barrier separating the Panthalassa Ocean from the continental interior (Keidel, 1925). This interpretation is now supported by recent studies that emphasize its role in modulating marine connectivity, sedimentation patterns, climatic belts, and biogeographic pathways across southern Gondwana (e.g., Bastos et al., 2021; Kern et al., 2021; Limarino et al., 2014, 2023a; Spalletti et al., 2010).

In the eastern intraplate sector, the intense and protracted deformation along the east–west–trending Ventana–Cape Fold Belt (~280 to post-250 Myr, Ramos et al., 2020, and references therein) most likely explains the intraplate isolation and eventual desiccation of the epicontinental sea through the closure of a possible seaway across southern Patagonia (Bastos et al., 2021) (Fig. 1b). It is further reinforced

* Corresponding author.
E-mail address: guidogianni22@gmail.com (G.M. Gianni).

https://doi.org/10.1016/j.epsl.2026.119920
Received 22 August 2025; Received in revised form 4 January 2026; Accepted 11 February 2026
Available online 28 February 2026

by Late Paleozoic-Mesozoic sea-level studies, which, despite some disagreement in magnitude, consistently indicate highstands during this period, reducing the likelihood that global sea-level fall was the primary driver of the Panthalassa Ocean regression (Haq and Cloetingh, 2025 and references therein) (Fig. 1c). Nevertheless, the progressive disconnection of the Panthalassa Ocean from multiple fore-, intra- and back-arc basins along the ancient western South American margin points to a far more complex paleogeographic evolution than can be explained by tectonic and/or eustatic sea-level change alone (Limarino et al., 2023a; Spalletti et al., 2010).

While orogenesis restricted marine ingressions, the complete disconnection and continentalization of the western active margin basins did not occur during peak orogenic activity, but rather during a subsequent phase of orogenic collapse (or extensional phase) between the mid-Permian and Early Triassic (~280–247 Ma, Limarino et al., 2023a, Spalletti et al., 2010; Sato et al., 2015; Fig. 1b). This seemingly

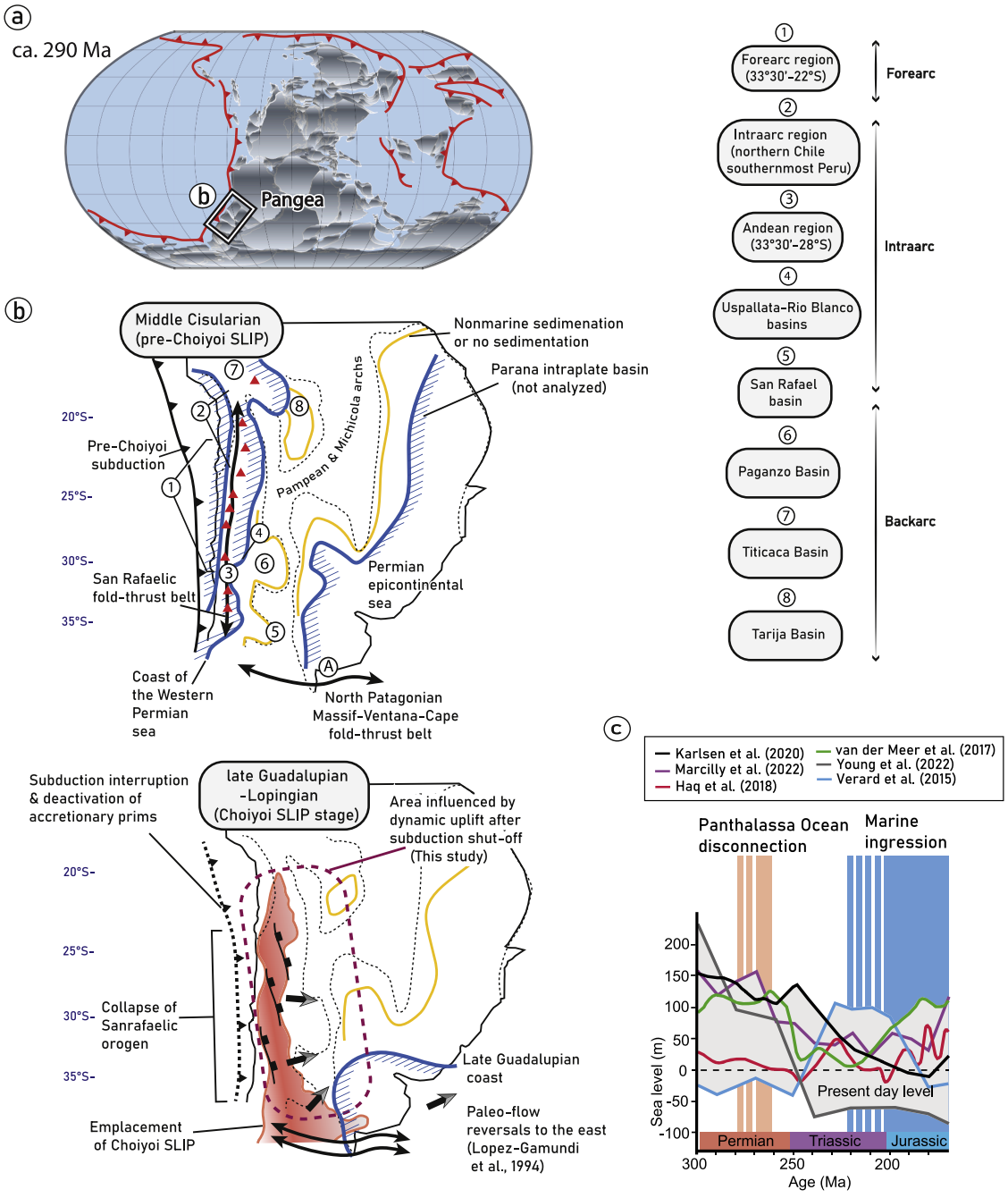

Fig. 1. a) Location of the study area (b) in southwestern Gondwana. b) Simplified paleogeographic maps of the study area for the mid-Cisuralian and the late Guadalupian-Lopingian, respectively (modified after Limarino et al., 2014). Numbers from 1 to 8 in b) indicate locations of Late Paleozoic basins analyzed in this study. The mid-Cisuralian reconstruction illustrates a restricted Panthalassan marine ingression across the western margin of Gondwana (Charrier et al., 2024; Díaz Martínez et al., 2000; Grader et al., 2008; Gutiérrez et al., 2018; Limarino et al., 2014, 2023a,b; Nina et al., 2020). In contrast, the late Guadalupian-Lopingian reconstruction depicts the complete marine disconnection between the Panthalassa Ocean and southwestern Gondwana, achieved between ~275 and 260 Ma, during the orogenic collapse phase associated with the emplacement of the Choiyoi silicic large igneous province (SLIP). c) Long-term sea-level reconstructions based on multiple methodologies, showing that despite notable discrepancies among models, most estimates suggest sea levels were higher than present during the time of full marine disconnection in the study area. This apparent paradox has led previous authors to propose a forced regression during the Late Permian (adapted from Haq and Cloetingh, 2025; Check this study for references to long-term sea-level curves shown in this panel).

counterintuitive timing (where the closure of marine gateways corresponds not to crustal shortening and uplift, but to lithospheric relaxation) challenges conventional assumptions and requires a re-evaluation of the mechanisms governing marine disconnection and continentalization along the southwestern margin of Gondwana.

To address this apparent paradox, we first examine the stratigraphic, tectonic, and paleogeographic evolution of Late Paleozoic basins along the southwestern margin of Gondwana. We then evaluate the potential role of dynamic topography generated by a major, progressive subduction interruption that occurred during the mid-Permian to Early Triassic in southwestern Gondwana (Arvizu et al., 2024; Gianni and Navarrete, 2022; Mpodozis and Kay, 1992). Using a simplified analytical model, we estimate first-order variations in dynamic topography associated with this event and contrast them with those expected under an alternative scenario of uninterrupted subduction (del Rey et al., 2019; Oliveros et al., 2020).

Finally, we discuss how this deep-Earth process may have contributed to the development of the orographic barrier responsible for the ultimate transition to fully continental conditions along the southwestern margin of Gondwana.

2. Records of Panthalassa ocean–southwestern Gondwana basin interactions along the pre-andean plate margin

2.1. Stratigraphy and tectonics of late Paleozoic basins in the southwestern Gondwana margin

Late Paleozoic basins of southern South America have been grouped into two main types: Eastern intraplate basins and plate margin-related basins, those aligned with the southwestern margin of Gondwana (presently the Andean region), both separated by intraplate highs (Michicola and Pampean arches, c.f. Limarino and Spalletti, 2006; Fig. 1b). Here, we focus on the latter (i.e., plate margin-related basins), providing a brief overview of the stratigraphic records documenting the evolution of Panthalassa Ocean–southwestern Gondwana connections across the following regions: forearc (sedimentary records spanning from 33°30′S to 22°S along the Chilean coast), intra-arc (depocenters along the current Chile–Argentina Central Andes, Titicaca, Calingasta-Uspallata–Río Blanco, and western San Rafael), and backarc basins (Paganzo, eastern San Rafael, and Tarija) (Fig. 1b). We also briefly review the associated tectonic and magmatic evolution of the active margin during the development of these basins (Fig. 2). An in-depth analysis of the eastern intraplate basins and the Ventana–Cape Fold Belt lies beyond the scope of this study, as the causes of marine disconnection in these regions are comparatively better understood (Bastos et al., 2021).

2.1.1. Late carboniferous-earliest permian

The influence of the Panthalassa Ocean during the Carboniferous to earliest Permian is evident in sedimentary records from basins along the western margin. These sedimentary records are characterized by glaciomarine sequences containing fauna of Panthalassan affinity (e.g., Barrealian fauna; Taboada, 2010); alongside terrestrial diamictite deposits that indicate a glacial phase in the late Visean to early Bashkirian. These are succeeded by postglacial marine transgressions, fossil-bearing sediments that reflect varied Panthalassan influence (e.g., Levipustula, Marginovatia, and Maemia faunas; Taboada, 2010), and by coal-bearing fluvial, alluvial, and estuarine deposits formed during the terminal glacial stage (Bashkirian to earliest Cisuralian) (Limarino et al., 2014 and references therein) (Fig. 2).

During the latest Mississippian-earliest Pennsylvanian (limit Serpukhovian/Bashkirian), glaciomarine and terrestrial diamictites were deposited in intra-arc depocenters of the Tarija (Macharetí and Mandiyutí Groups) and Calingasta–Uspallata (Hoyada Verde Formation and equivalents) basins, and as well as in the backarc Paganzo (Guandacol Formation and equivalents) and San Rafael (base of El Imperial

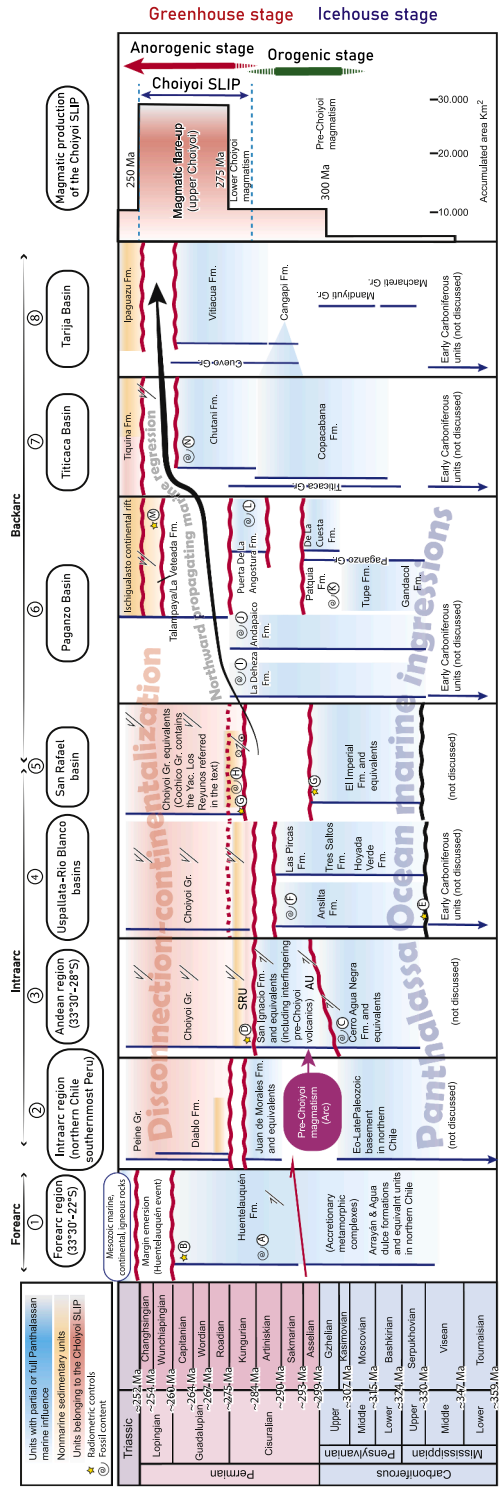

Fig. 2. Stratigraphy of the major late Paleozoic basins analyzed in this study based on a synthesis of previous literature (Charrier et al., 2024; Díaz-Martínez et al., 2000; Grader et al., 2008; Gulbranson et al., 2015; Gutiérrez et al., 2018; Kleiman and Japas, 2009; Limarino et al., 2014, 2023a,b; Nina et al., 2020; Rocha-Campos et al., 2011; Vicente et al., 2005). Choiyoi magmatic province data is from Bastías-Mercado et al. (2020). Age constraints based on radiometric ages and fossil content are: A: Díaz-Martínez et al. (2000); B: Bahlburg et al. (2009); C: Limarino et al. (2023a); D: Sato et al. (2015); E: Malone et al. (2024); F: Césari et al. (2014); G: Rocha-Campos et al. (2011); H: Vézquez and Césari (2017); Balarino et al. (2016); Gutierrez et al. (2018); Balarino et al. (2012); Gutierrez et al. (2018); K: Archangelsky and Cuneo(1987); L: Césari et al. (2022); M: Bernardez et al. (2023); N: Iannuzzi et al. (2004). Abbreviations are SRU: San Rafael Unconformity and AU: Atacama Unconformity.

Formation) basins. In the Middle Pennsylvanian, these units are overlain by early Pennsylvanian (Bashkirian) postglacial transgressive shales, followed by deltaic and fluvial deposits (Limarino and Spalletti, 2006, and references therein) (Fig. 2).

During the latest Carboniferous to early Permian, the southwestern Gondwanan margin experienced a dynamic interplay of sedimentation, magmatism, and tectonics, reflecting a transitional geodynamic regime. In the Paganzo Basin, backarc sedimentation is recorded by the Patquía Formation and equivalents, which consists of fluvial sandstones and conglomerates transitioning upward into ephemeral river, playa lake, and eolian facies, indicating increasing aridity and continentality (Spalletti et al., 2010) (Fig. 2). Pennsylvanian to early Permian strata in the Río Blanco and Calingasta–Uspallata basins, to the west, are preserved in transitional to shallow marine siliciclastic facies (e.g., Tres Saltos, Agua del Jaguel, Ansilta and Del Salto formations) (Fig. 2). In the Andean sector, minor diamictites within the Cerro Agua Negra Formation and its equivalents (e.g., the Late Carboniferous–Early Permian El Imperial Formation in western San Rafael) were deposited in nearshore to offshore environments, attesting to persistent marine influence in these intra-arc depocenters (Fig. 2). To the north, in the Tarija backarc basin, Late Pennsylvanian–Early Cisuralian sedimentation is represented by the Mandiyutí Group (Escarpment and San Telmo formations), recording fluvial to deltaic environments in the lower section and shallow marine and coastal environments conditions, including possible diamictites in shallow lakes in the upper section (Limarino and Spalletti, 2006). In the Titicaca backarc basin, an important latest Carboniferous–Early Permian transgression is preserved in the lower Copacabana Formation, with shallow marine, deltaic, and fluvial siliciclastic deposits (Grader et al., 2008) (Fig. 2).

In the forearc region, active subduction during the Late Carboniferous–Early Permian is evidenced by the formation of accretionary prisms composed of deformed and metamorphosed turbiditic sequences (e.g., Arrayán Formation and equivalents) (Charrier et al., 2024). Coeval arc magmatism is represented by calc-alkaline batholiths and minor volcanics associated with pre-Choiyoi magmatism, confirming the existence of an active continental margin at this time (Hervé et al., 2014; Sato et al., 2015) (Figs. 1b and 2). This pre-Choiyoi arc has been linked to the onset of compressive tectonics during the latest Carboniferous to earliest Permian, marking the first orogenic phase in proto-Andean uplift (e.g., García-Sansegundo et al., 2014). The tectonic expression of this phase is particularly well recorded in Late Paleozoic depocenters along the Andean belt, most notably through syn-sedimentary contractional deformation and subaerial exposure of the preserved in the upper Cerro Agua Negra and lower San Ignacio formations (Busquets et al., 2005; Limarino et al., 2023a) (Fig. 2). These features define a prominent regional unconformity attributed to the Atacama orogenic phase, marking the shift from offshore to dominantly continental and shallow marine deposition (Limarino and Spalletti, 2006; Limarino et al., 2014; 2023a and references therein) (Fig. 2).

2.1.2. Early permian-early triassic

During the Early Permian (middle Cisuralian), siliciclastic sedimentation was progressively replaced by carbonate deposition in shallow marine and coastal lagoonal settings, closely linked to the development of the pre-Choiyoi magmatic arc. This transition reflects a broader climatic shift from the cool, periglacial conditions of the Carboniferous to the warmer climates of the early Permian (Limarino et al., 2014). The change is recorded in shallow marine deposition in intra-arc depocenters, particularly in the upper San Ignacio, Castaño Viejo, and Juan de Morales formations, as well as in equivalent units such as the upper Copacabana, Cerro Oscuro, Cerro del Árbol, Arizaro, and Cerros de Cuevitas formations (Artinskian ± Kungurian; Busquets et al., 2013; Césari et al., 2011; Díaz-Martínez et al., 2000; Grader et al., 2008) (Fig. 2).

These strata are considered partial equivalents of the lower sections of the fossiliferous neritic marine deposits of the Huentelauquén Formation and its forearc correlatives, which contain diagnostic microfossils and a maximum depositional zircon age that together constrain them to the late Cisuralian to early Lopingian (Díaz-Martínez et al., 2000; Charrier et al., 2024 and references therein) (Fig. 2). In addition, portions of these sedimentary units reflect a significant tectonic episode along the active margin. This is evidenced by the presence of syn-contractional growth strata and intraformational unconformities within synorogenic piggyback basins that developed during forelandward propagation of the orogenic wedge, particularly in the upper San Ignacio, Castaño Viejo, and equivalent units (Busquets et al., 2005, 2008; e.g., Del Salto-Quebrada del Alumbre formations of Colombo et al., 2014; Limarino et al., 2023a). This stage marks a critical moment in the tectonic evolution of southwestern Gondwana, culminating in the development of the regional San Rafael unconformity (Fig. 2). This erosive surface separates deformed Late Paleozoic units from overlying formations deposited on an irregular paleotopography and signals both the onset of the mid-Cisuralian–Early Triassic Choiyoi SLIP and the end of the Gondwanide orogenic phase (Sato et al., 2015) (Figs. 1b and 2).

The Choiyoi SLIP comprises predominantly mesosilicic to silicic volcanic rocks and exhibits a compositional evolution from calc-alkaline or transitional types in its lower part to more alkaline rocks in its upper levels (Sato et al., 2015). The initial phase of magmatism began around 286–280 Ma, followed by a major flare-up between approximately 275 and 250 Ma, during which nearly 75 % of the SLIP volume emplaced (Bastías-Mercado et al., 2020) (Fig. 2). Early volcanic products include fluvial-alluvial coarse-grained deposits, eolian sediments, and lacustrine facies that were progressively replaced by extensive silicic volcanic and volcaniclastic successions (Mancuso et al., 2016; Strazzere et al., 2016; Rocha-Campos et al., 2011).

With the exception of localized transpressional deformation mostly observed in the western San Rafael Basin, Choiyoi volcanism was predominantly emplaced under extensional to transtensional tectonic conditions (Fig. 2). The volcanic architecture was largely influenced by normal fault systems, creating in some cases ~2–5 km deep depocenters, and is spatially associated with elongated plutonic bodies and dyke swarms (Sato et al., 2015; ; Busquets et al., 2005; Cristallini and Ramos, 2000; Heredia et al., 2002; Giambiagi et al., 2011; Heredia et al., 2012). Accordingly, this phase reflects the tectonic shift from compressional Gondwanide orogeny to a broadly extensional, anorogenic regime (Sato et al., 2015).

Restricted marine connections with the Panthalassa Ocean persisted into the initial stages of Choiyoi SLIP activity, when magmatic output was still minimal. This is evidenced by sedimentary records indicating marine influence during the extrusion of lower Choiyoi magmatism. For example, the Andapaico and La Dehesa formations record foreshore, barrier island, and lagoonal environments in their upper sections, consistent with shallow marine conditions during the Cisuralian (see Gutiérrez et al., 2018 and references therein) (Fig. 2). Other contemporaneous units with volcaniclastic input interpreted as derived from the Choiyoi SLIP include the upper Puerta de las Angosturas Formation (Paganzo Basin), the Vitiacua Formation (Tarija Basin), and the Chutani Formation (Titicaca Basin), all indicating restricted shallow marine settings in different sections (Grader et al., 2008; Limarino et al., 2014, 2023b; Nina et al., 2020 and references therein) (Fig. 2). These successions are time-equivalent to the uppermost shallow marine Huentelauquén Formation and were partially correlated based on microfossil assemblages (Díaz-Martínez et al., 2000) (Fig. 2).

Complete marine disconnection from the Panthalassa Ocean occurred during the later stages of the Choiyoi SLIP, when the accumulation of thick volcanic sequences, comprising lava flows, ignimbrites, and tuffs, effectively curtailed sedimentation, with only minor deposition during inter-eruptive intervals (Limarino et al., 2014) (Fig. 2). We note that this turning point in the evolution of the Panthalassa–Gondwana margin coincided with the Choiyoi SLIP flare-up phase after ~275 Ma, when most of the magmatism was emplaced (late Kungurian–Roadian; Bastías-Mercado et al., 2020) (Fig. 2).

In the eastern backarc region, Permian sedimentation ceased in basins such as Titicaca and Tarija, or was dominated by nonmarine facies including fluvial conglomerates and sandstones, exemplified by the Talampaya and La Veteada formations in the Paganzo Basin and possibly the slightly older Yacimiento Los Reyunos Formation in the San Rafael Basin (Fig. 2). These nonmarine units, dated to the latest Permian (late Kungurian–Changhsingian), reflect increasingly arid and seasonal conditions, as supported by sedimentary facies and palynological data (Gulbranson et al., 2015; Gutiérrez et al., 2018; Rocha-Campos et al., 2011) (Fig. 2).

In the forearc region, this disconnection is marked by a regional uplift known as the Huentelauquén event (sensu Charrier et al., 2024). This is represented by a latest Permian unconformity that separates the Carboniferous Arrayán and early to middle Permian Huentelauquén formations from overlying marine Triassic strata, indicating a halt in sedimentation and widespread continental emergence along the margin (Charrier et al., 2024) (Fig. 2). Paleoclimatic changes during the middle Permian, particularly the onset of continental aridity, have been attributed to the emergence of an orographic barrier related to the Choiyoi SLIP. This barrier would have hindered moisture inflow from the Panthalassa Ocean under a globally warming climate (Spalletti et al., 2010), resulting in the widespread development of eolian dune fields interpreted as sand seas (Mancuso et al., 2016).

2.2. Tectono-magmatic controls on Panthallasan marine disconnection

Accumulating evidence indicates that orogenic activity during the latest Carboniferous to Early Permian exerted control on marine connectivity with the Panthalassa Ocean, partially restricting transgressive episodes. Marine incursions, frequent during the early to late Early Carboniferous, became progressively less common by the latest Carboniferous - earliest Permian and were reduced during the mid-Cisuralian (late Early Permian), when topographic uplift increasingly acted as a barrier to marine inflow (Limarino and Spalletti, 2006; Limarino et al. 2023a) (Figs. 1b and 2). However, this orogenic activity appears to have produced only moderate topographic relief. This is evidenced by the continued presence of shallow marine to transitional synorogenic deposits adjacent to the active magmatic arc and, in some cases, extending into the back-arc region (Busquets et al., 2005, 2013; Limarino et al., 2014, 2023a; Fig. 2).

These geological observations challenge recent crustal thickening estimations based on geochemical proxies (ca. 46 km, 280–253 Ma, Alasino et al., 2022) and derived paleoelevation analyses (Liu et al., 2024). The latter suggest that during the Late Carboniferous to Permian (330–250 Myr), elevations across the study area (40°–20°S) generally exceeded 2500 m, with localized estimates reaching orogenic plateau-like heights of up to 5000 m (see Figure 7 in Liu et al., 2024). These estimates, indicating heights and crustal thicknesses comparable to the Patagonian or northern Andes (1500–3500 masl, 40–45 km), are incompatible with well-documented evidence from intra-arc depocenters (e.g., modern Chile–Argentina Central Andes, Titicaca, Uspallata–Río Blanco, and western San Rafael regions) of offshore to shallow marine siliciclastic sedimentary records from the pre-orogenic stage up to 300 Ma (e.g., Cerro Agua Negra, El Imperial, Hoyada Verde, Tres Saltos, Sierra del Tigre formations; Fig. 2). More critically, paleoelevations conflict with the record of syn-tectonic sedimentation at or near sea level along the orogenic hinterland between 290 and 280 Ma (Artinskian ± Kungurian; Busquets et al., 2005; Colombo et al., 2014, 2013; Limarino et al., 2014, 2023a; Fig. 2). Moreover, as stated above, shallow marine facies were reported in different parts of the back-arc from 40°–20°S following the San Rafael unconformity during the early stages of Choiyoi SLIP magmatism (Grader et al., 2008; Limarino et al., 2014, 2023b; Nina et al., 2020; Fig. 2). These key observations illustrate the limitations of deriving crustal thickness estimates from geochemical proxies and underscores the critical importance of considering the sedimentary basin record when applying such techniques. A possible explanation for the mismatch between geochemical proxies for crustal thickness and paleoaltimetry and the sedimentary record is that previous studies assumed a purely subduction-related origin for the Choiyoi SLIP (i.e., magmas derived from the mantle wedge and fractionated at high pressure near Moho depths). This assumption overlooks potential contributions from melts sourced directly from the subducted plate, which can produce similar geochemical signatures but do not record paleo–Moho depths. Such melts can be formed during slab detachment events (Gianni and Navarrete, 2022; Whalen and Hildebrand, 2019; next section).

Collectively, these observations suggest that while crustal thickening associated with early orogenic processes restricted marine ingressions along the western active margin, it cannot account for the complete disconnection from the Panthalassa Ocean. The progressive desiccation of basins along the southwestern margin of Gondwana could also reflect large-scale global processes. While some studies report a global sea-level drop near the Permian–Triassic boundary (~250 Ma), these values remain above present-day levels and postdate the main marine regression in the study area, largely completed by ~275–265 Ma (Fig. 2). Other reconstructions suggest a sea-level rise of 20–150 m above modern levels during this interval (Haq and Cloetingh, 2025 and references therein; Fig. 2). Hence, directly linking the marine regression to Late Paleozoic sea-level dynamics is difficult.

Limarino et al. (2014, 2023a) and Spalletti et al. (2010) noted a temporal coincidence between the onset of full marine disconnection and the emplacement of the Choiyoi SLIP during orogenic collapse of the southwestern Gondwanan margin, a phase dominated by crustal stretching and extensional magmatism. These observations raise a critical unresolved question: How could the final disconnection of the Panthalassa Ocean from the southwestern margin of Gondwana occur during a phase of lithospheric thinning and postglacial sea levels likely well above present-day?

2.3. Origin of the Choiyoi SLIP

Two end-member hypotheses have been proposed to account for the development of the Choiyoi Magmatic Province. The first hypothesis proposes an origin entirely (Mpodozis and Kay, 1992) or partly (e.g., upper Choiyoi; Kleiman and Japas, 2009) linked to a cessation of subduction, triggered by slab break-off events.

The second hypothesis suggests a scenario of continued subduction accompanied by slab rollback within a retreating subduction system (e.g., del Rey et al., 2019; Oliveros et al., 2020). The continued-subduction model relies primarily on geochemical evidence indicating that the lower Choiyoi magmatism, and more locally the upper section (González et al., 2025), exhibit a subduction-related signature (e.g., Bastías-Mercado et al., 2020). Recent studies have proposed that this geochemical signature may be entirely inherited (post-subduction magmatism), and have documented geochemical fingerprints associated with slab break-off (Gianni and Navarrete, 2022). Notably, seismic tomography reveals lower-mantle slab remnants of Permian subduction only to the north and south of the reconstructed position of the Choiyoi SLIP, where a major slab gap is present, an observation incompatible with sustained plate convergence beneath the region (Arvizu et al., 2024; Gianni and Navarrete, 2022). More critically, documentation of spatio-temporal patterns of magmatism showing inland migration of up to 300–500 km contradicts slab-rollback models, which typically produce trenchward magmatic retreat (e.g., Gianni and Pérez-Lujan 2021). Subduction interruption is further corroborated by recent geochronological data suggesting the deactivation and subsequent emergence of accretionary complexes between 33° and 22°S, linked to the Huentelauquén event, which occurred sometime between the Late Permian and pre-Early Triassic (Charrier et al., 2024). Taken together, these independent lines of evidence challenge a subduction-related origin for the Choiyoi SLIP and instead support a scenario of progressive, regionally extensive subduction shutdown between ~275 and 250

Ma (Arvizu et al., 2024; Gianni and Navarrete, 2022; Kleiman and Japas, 2009; Mpodozis and Kay, 1992).

Slab break-off events and their subsequent detachment can induce the partial melting of the upper portion of the eclogitized or partially eclogitized oceanic crust through rapid temperature increases during slab foundering (Whalen and Hildebrand, 2019). Thus, the partial melting of subducted metabasaltic and metasedimetary components results in intermediate-felsic magmas, geochemically characterized by a variable HREE depletion, moderate to high $^{87}Sr/^{86}Sr$, and high Th/La values (Whalen and Hildebrand, 2019). As indicated by Gianni and Navarrete (2022), the Choiyoi SLIP filtered geochemical dataset exhibits a general slab break-off signature by HREE depletions. These authors indicated that most of the Choiyoi SLIP was related to the partial melting of subducted components. In this regard, the moderate to high $^{87}Sr/^{86}Sr$ values (from 0.7033 to 0.72285; average: 0.7086) of this magmatic province show a constant, relatively flat pattern as SiO2 increases, which inhibits attributing such magmatic evolution to crustal assimilation (Fig. 3). Considering the general geochemical features described by Gianni and Navarrete (2022), this isotopic signature is likely inherited from its source and is consistent with the isotopic compositions of subducted metabasaltic and metasedimentary components (e.g., Zhang et al., 2024); it is therefore not necessarily indicative of a typical subduction-related mantle-wedge source (e.g., González et al., 2025; Oliveros et al., 2020). Lastly, the massive volumes of silicic magmatism during slab break-off would have been facilitated by Pangea supercontinent thermal insulation that raised upper mantle potential temperatures in excess of 150 °C (Brandl et al., 2013).

Noteworthy, the different hypotheses suggested for the Choiyoi SLIP have contrasting dynamic topography signatures [i.e., lithospheric deflections caused by mantle flow; Hager and O'Connell, 1979], and hence, testable implications for the Permian–Triassic paleogeography of southwestern Gondwana. While geodynamic settings involving active subduction would be associated with dynamic subsidence along the plate margin (e.g., Hager and O'Connell, 1979; Hoggard et al., 2016), scenarios invoking subduction interruption would lead to the development of relative dynamic uplift (Davies and von Blanckenburg, 1995). These contrasting dynamic responses are worth considering, as they may hold a potential explanation for the enigmatic marine disconnection between the Panthalassa Ocean and active-margin basins during the Permian–Triassic transition.

3. Dynamic topography analysis

To incorporate potential dynamic topography effects in the paleogeographic evolution of southwestern Gondwana, we implemented an analytical model that simulates the instantaneous dynamic topography produced by subducting slabs of variable geometry, density contrast, and mantle viscosity. The model is based on the classical analytical framework of Hager and O'Connell (1979), with subsequent refinements (e.g., Gurnis et al., 2000; Ricard et al., 1984). It assumes creeping Stokes flow in a Newtonian viscous mantle, where vertical normal stresses are exerted on the base of the lithosphere by buoyancy forces arising from internal density anomalies such as slabs. The slab is discretized, and its depth and geometry are integrated into the surface stress computation. Dynamic topography, h(x,y), is estimated as the surface deflection resulting from vertical normal stresses generated by subducting slabs in a viscous mantle. For a Newtonian fluid under creeping flow, the deflection scales with the buoyancy force per unit area divided by the resistance of the mantle to flow, leading to the simplified expression:

$$\mathbf{h}(\mathbf{x},\mathbf{y}) = -\left[\Delta\rho(\mathbf{x},\mathbf{y})\cdot\mathbf{g}\cdot\mathbf{D}(\mathbf{x},\mathbf{y})^2\right]/\eta(\mathbf{x},\mathbf{y})$$

Where Δρ(x,y) is the local density anomaly (typically 60–100 kg/m^3), g is gravitational acceleration (9.81 m/s^2), D(x,y) is the slab depth, and η(x,y) is the effective mantle viscosity. The quadratic dependence on depth reflects the integration of buoyancy forces over the vertical extent of the slab. This formulation follows classical scaling relationships for instantaneous viscous flow (e.g., Hager and O'Connell, 1979). To parameterize the density field, the radial stress is first computed as:

$$\sigma_{rr}(x,y) = (\Delta\rho\cdot g\cdot d)/r^2$$

where *d* is the depth of the slab segment and *r* is the horizontal distance from a surface point to the slab element. We assume $\Delta\rho = 90\cdot\sin(\theta)$ kg/m^3 as a first-order proxy for slab buoyancy, with θ representing the slab dip angle. Contributions from slab segments below the 660 km mantle discontinuity are neglected due to their limited influence on surface stresses.

We implemented a simplified dynamic topography model constrained by sectoral variations in slab geometry and mantle rheology. The modeled domain spans 3000 km in the east–west direction and 3500 km north–south, discretized into a 100 × 100 grid. Slab geometries were prescribed independently for the Northern, Central, and Southern

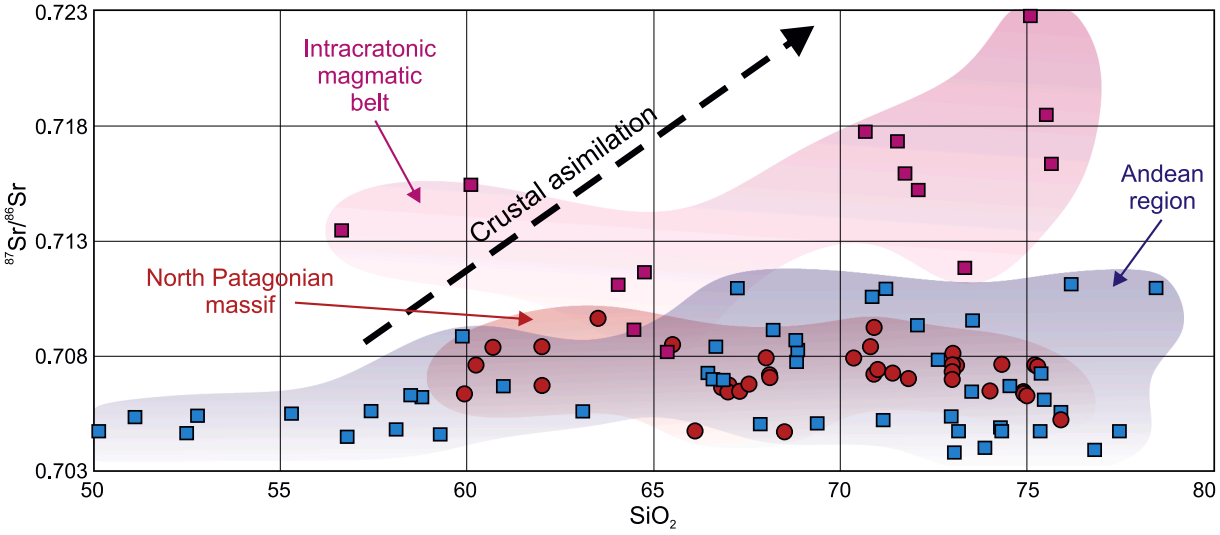

Fig. 3. $^{87}Sr/^{86}Sr$ vs SiO_2 diagram of Choiyoi SLIP. Note the relatively flat patterns of $^{87}Sr/^{86}Sr$ as SiO2 increases, precluding attribution of the magmatic evolution by crustal assimilation. Intracratonic magmatic belt, Andean region, and North Patagonian Massif refer to the three main regions of the Choiyoi SLIP. Data compilation is from: Pankhurst et al. (2006); Sato et al. (2000); del Rey et al. (2019); Compiled data in Dopico et al. (2019); López de Luchi et al. (2021), and González et al. (2025).

sectors and also include slab break-off scenarios (absence of slab). Density and viscosity values were scaled per sector using empirical functions of slab dip.

In the absence of precise constraints on slab age during the Permian–Triassic, we adopted average density anomalies representative of typical subducting lithosphere. A sensitivity analysis (Figure S1, Supplementary Material) explores a plausible range of viscosity and density contrast scenarios. Additionally, variations in mantle viscosity between continuous and interrupted subduction scenarios are introduced to simulate changes to relatively hotter mantle conditions that would occur following subduction shutdown. This approach highlights the relative effects of transitioning from active subduction to its interruption, rather than relying on absolute magnitudes tied to poorly constrained physical parameters.

To test alternative hypotheses regarding the subduction history of southwestern Gondwana, we evaluated two end-member scenarios (1 and 2; see below), each considering different subduction geometries proposed for two plausible configurations during the Late Carboniferous–Early Permian (hereafter scenarios Permian 1 and Permian 2), as well as a comparable Late Permian–Early Triassic configuration (Early Triassic) (Fig. 4a-e).

3.1. *Latest Carboniferous–Early Permian (or Permian 1) stage vs. late Permian–Early Triassic (or early triassic) stage*

In the Permian 1 stage, continuous subduction occurs along the entire pre-Andean margin from north to south. Slab dip angles were set at 30° for the northern (0°–18°S) and southern (40°–55°S) margin segments, and at a shallow angle of 10° for the central segment (15°–40°S), following García-Sansegundo et al. (2014) (Fig. 4a). In contrast, the Early Triassic stage (Fig. 4b) introduces a slab gap in the central segment, representing a zone of subduction interruption. This large gap is intended to reflect the Late Permian–Early Triassic subduction cessation, coinciding with the magmatic flare-up of the Choiyoi SLIP (~275–250 Ma) and the generalized slab break-off stage (; Arvizu et al., 2024; Gianni and Navarrete, 2022). For both the northern and southern segments, the slab dip remains unchanged during the Late Permian–Early Triassic (Early Triassic scenario). The resulting dynamic topography differences between stages are illustrated in Fig. 4d

3.2. *Alternative latest Carboniferous–Early Permian (or Permian 2) stage vs. Late Permian–Early Triassic (or Early Triassic) stage:*

This second comparison explores an alternative configuration for the Latest Carboniferous–Early Permian stage. In this stage of Permian 2 (Fig. 4c), we used the same slab dip in the northern and southern segments as in Stage Permian 1 and tested an alternative 30° slab dip for the central margin segment, which accounts for the rather limited Permian arc migration recorded in this latitudinal sedment, which can be alternatively caused by subduction erosion or other processes instead of changes in slab dip (see Gianni and Perez-Lujan 2021). Then, Fig. 4c can be considered as testing the overall effect of the continued subduction hypothesis across the entire time spam analyzed (Late Carboniferous to Early Triassic, del Rey et al., 2019; Oliveros et al., 2020). We acknowledge that alternative slab-dip geometries have been proposed for the southern segment (e.g., flat subduction; Pysklywec and Mitrovica, 1998). However, testing their potential dynamic effects (e.g., Liu et al., 2008) lies beyond the scope of this study, as our analysis focuses specifically on the dynamic-topography implications of active versus inactive subduction beneath the central Andean region. The corresponding change in dynamic topography for these stages is presented in Fig. 4e.

For the reference subduction scenarios, our model predicts different outcomes depending on whether the dynamic topography effects of continuous or interrupted subduction are considered in the central segment of the study area. As expected, the overall effect of a normal dipping active subduction process (uninterrupted subduction model: Oliveros et al., 2020) is a broad region (1000–1500 km wide) of dynamic subsidence (~0.7 km) near the active margin (e.g., Ricard et al., 1984; Gurnis et al., 2000) (Fig. 4c). Such a dynamically subsiding setting is difficult to reconcile with the documented regional marine regression and the disconnection of active-margin basins from the Panthalassa Ocean, particularly given the documented regional extension(del Rey et al., 2019) (Fig. 2). In contrast, considering a subduction interruption in the central segment produces a zone of relative dynamic uplift, associated with the loss of dynamic support (Figs. 4d and e; also

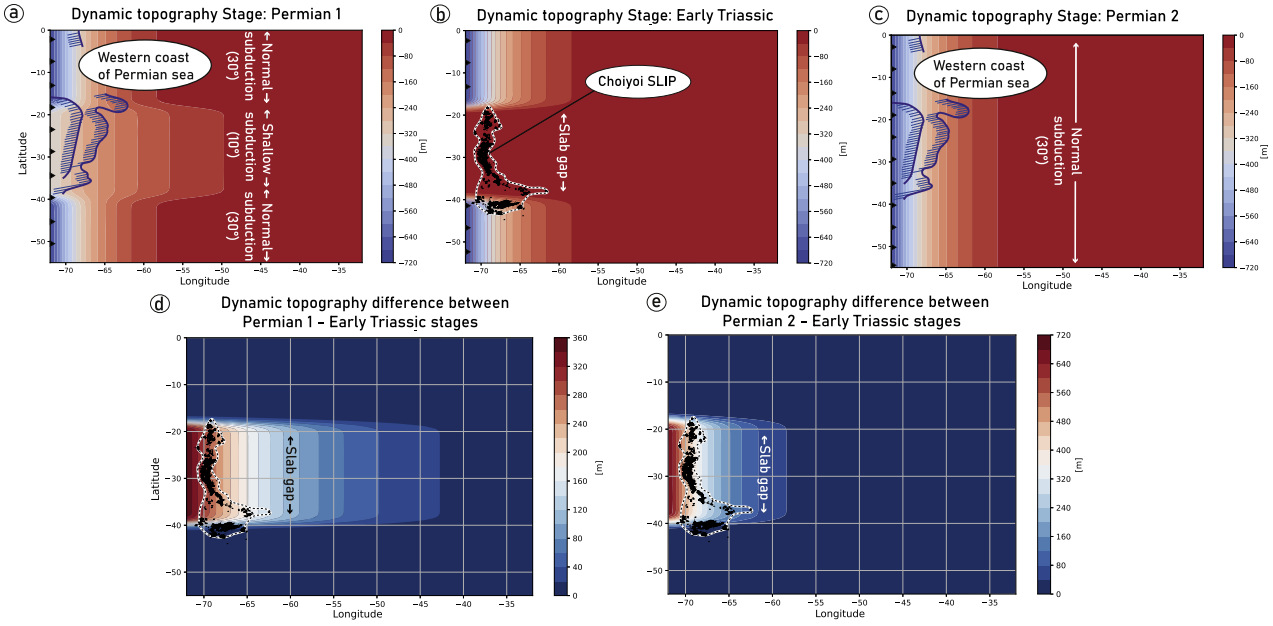

Fig. 4. Dynamic topography analysis during a subduction-to-subduction interruption process. (a), (b) and (c) maps show interpolated values on instantaneous dynamic topography (models Permian 1, Early Triassic, and Permian 2) computed using the Hager and O'Connell (1979) approach. (d) and (e) maps illustrate the change of dynamic topography (Permian1-Early Triassic and Permian 2-Early Triassic, respectively) by subtracting a and b and c and b. The coordinates are respect to modern coordinates. Viscosities: Slab = $1e^{21}$, Mantle = $1e^{20}$, Hot mantle = $1e^{19}$.

observed in alternative scenarios, see Supplementary Material, Figure S1). In our reference model, this uplift exhibits broad long-wavelength signals of ~1000–2000 km and amplitudes of approximately 0.4–0.7 km when we use average viscosity and density contrast values, well within the range of dynamic topography values observed in modern settings (Hoggard et al., 2016) (alternative viscosity and density scenarios show variable uplift amplitudes; see Figure S1). The uplifted region extends from the Chilean trench across the forearc and into the distal back-arc region suggesting that subduction interruption may have exerted a first order control on surface elevation along the margin (Figs. 2, 4d, and e; see Supplementary Material, Figure S1).

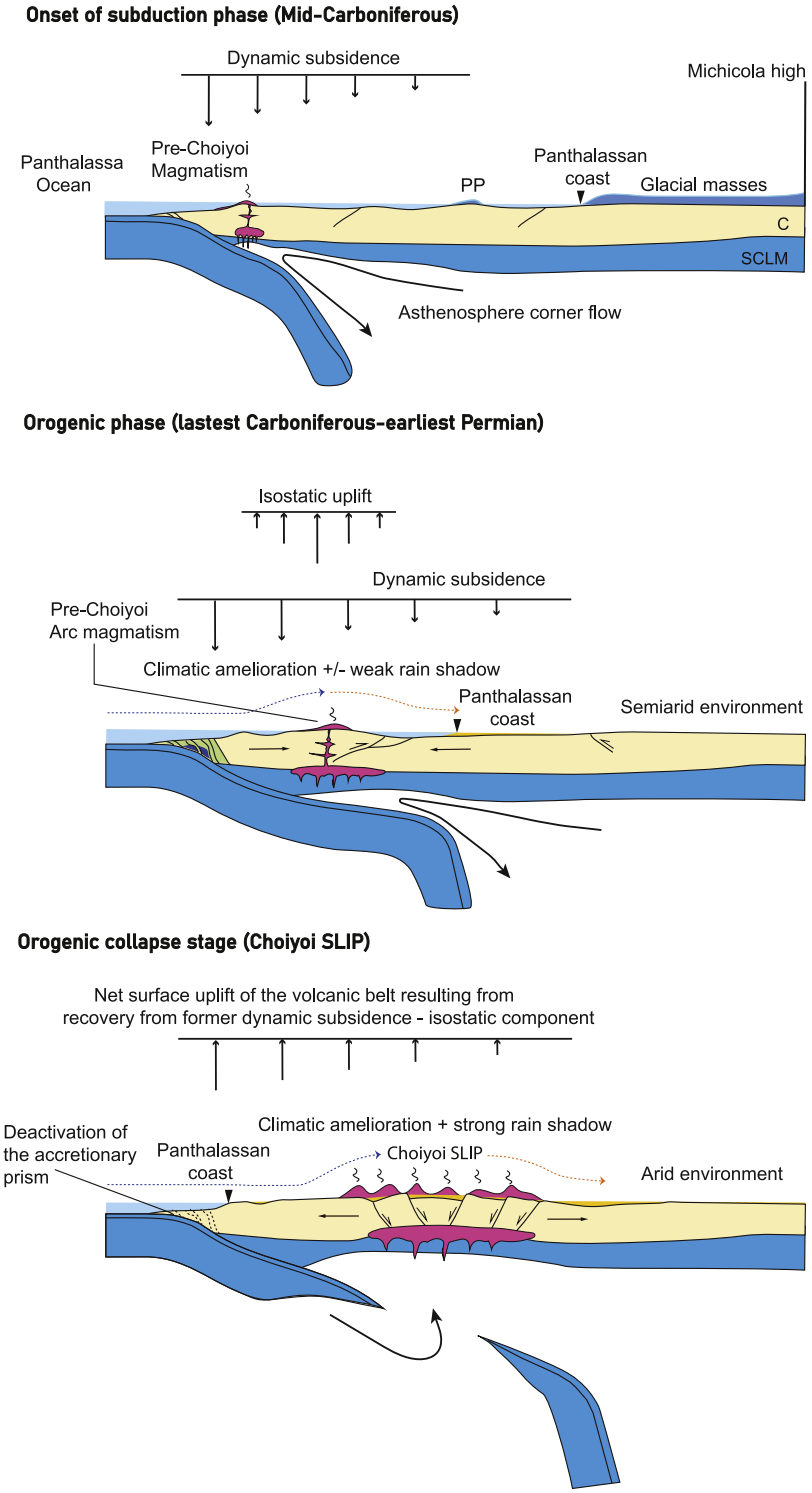

Fig. 5. Schematic model illustrating the progressive restriction and final closure of Panthalassan marine ingressions into the southwestern interior of Gondwana. Early orogenic activity played a key role in narrowing marine inlets, while later dynamic surface uplift, triggered by the interruption of subduction, ultimately blocked marine connections entirely. Abbreviations are; C: Continental crust; SCLM: Subcontinental lithospheric mantle, and PP: Proto-Precordillera high.

4. Discussion and conclusions

The paleogeographic evolution of southwestern Gondwana during the Late Paleozoic is often viewed through the lens of orogenic processes and climate transitions (Keidel, 1925; Limarino et al., 2014). While the role of the Gondwanide orogeny in modulating marine ingressions is well established (Bastos et al., 2021; Kern et al., 2021; Limarino et al., 2023a), our analysis reveals that this narrative is incomplete without integrating deep mantle dynamics (see Pysklywec and Mitrovica, 1998), specifically, the impact of a regional-scale subduction interruption along the western proto-Andes margin and its consequences on surface topography. As outlined above, a key unresolved issue is that stratigraphic records from forearc, intra-arc, and back-arc regions consistently indicate that full disconnection from the Panthalassa Ocean was contemporaneous with global deglaciation and postdated peak Early Permian orogenesis (Figs. 1b and 2). Considering the conservative pre-286 Ma timing for the end of the San Rafael orogenic phase along the proto-Andean margin based on the oldest Choiyoi SLIP age in this region (Sato et al., 2015), and the ages of units preserving the last restricted shallow marine deposits (Juan de Morales, Andapaico, La Deheza, Formación Puerta de las Angosturas, and Chutani formations; Grader et al., 2008; Gutiérrez et al., 2018 and references therein; Limarino et al., 2023b; Nina et al., 2020), the complete disconnection from the Panthalassa Ocean and resulting continentalization occurred >10 million years after the orogenic phase (Fig. 2). Particularly intriguing is that this process unfolded during a progressive shift toward extension and transtension, a phase of tectono-magmatic reorganization associated with the Choiyoi SLIP, rendering the overall scenario counterintuitive from an isostatic perspective. Although the magnitude of crustal extension has not yet been fully quantified, its isostatic effect would have reduced regional elevation. Under sea levels higher than present (Haq and Cloetingh, 2025; Fig. 2), this would have favored the persistence of marine inlets connecting to the Gondwanan interior.

Our study reframes this timing not as a tectono-stratigraphic anomaly, but as the surface expression of a profound change in subduction regime. Our simple dynamic topography models, despite their limitations, offer an explanatory mechanism for regional topography. A continuous Permian-Triassic subduction scenario, creates broad dynamic subsidence (~0.7 km), which is difficult to reconcile with the documented regional marine regression (Fig. 4c). In contrast, models of subduction interruption show that removing the dynamic subsidence generated by a subducting slab produces long-wavelength, margin-scale relative surface uplift (Fig. 4d,e), with predicted amplitudes of ~0.4–0.7 km and wavelengths of ~1000–2000 km, values consistent with natural dynamic topography. Such uplift is sufficient to disrupt shallow seaways (e.g., Garcia-Castellanos and Villaseñor, 2011), creating physiographic barriers that could have contributed to the final isolation of western basins along the southwestern margin of Gondwana (Fig. 5).

Indirect evidence for a phase of surface uplift coinciding with the Choiyoi flare-up is supported by multiple lines of observation. Sandstone compositional analyses, used to infer source rock types, combined with paleocurrent data indicating sediment transport directions, led López-Gamundí et al. (1994) (see Fig. 13 in this study) to identify a major shift in provenance and paleo-drainage across the three best-studied western depocenters: Calingasta–Uspallata, San Rafael, and Paganzo Basins. According to these authors, this shift reflects the increasing influence of Choiyoi-related volcanism and a reversal of the regional slope and drainage direction, generally toward the east-northeast (Fig. 1b; late Guadalupian–Lopingian stage).

The change in paleo-slope, interpreted here as the result of surface uplift driven by subduction interruption, is further supported by U–Pb detrital zircon provenance analyses in the intraplate Paraná Basin from Late Permian [Kungurian (marine)–Wuchiapingian (continental)] sedimentary units (Kern et al., 2021). These data show an abrupt influx of Famatinian cycle-age (~369–484 Ma) zircons during the latest Permian, indicative of uplift and erosion of basement rocks along the western Gondwana margin, with minor contributions from exhumed western Late Paleozoic basins. While Kern et al. (2021) linked southern zircon sources to the Gondwanic Ventana–Cape Fold and Thrust Belt and the North Patagonian Massif, these authors did not fully explain the origin of the uplifting region driving the exhumation of Famatinian cycle igneous–metamorphic complexes in the west or the reworking of sediments from uplifted western basins. Our results provide a viable mechanism for this enigmatic surface uplift to the west, despite the predominantly anorogenic setting of the proto-Andean margin at the time, through dynamic surface response to subduction interruption. In addition, this process could explain the scarce sedimentary record of the middle to upper Permian in the back-arc and distal back-arc regions (Limarino and Spalletti, 2006). Also, our results offer a complementary mechanism for Late Permian aridification of the continental interior, a phenomenon Spalletti et al. (2010) and Limarino et al. (2014) attributed to the piling-up of volcanic materials creating a topographic high during Choiyoi SLIP emplacement. In their model, this orographic barrier forced humid Panthalassan winds to rise and release moisture along the coast, amplifying inland aridity (Fig. 5).

To generate a pronounced rain shadow over the study area, the orographic barrier would have needed to reach elevations of at least ~1 km (e.g., Bucher et al., 2020). However, the geological record suggests that such high-standing relief was unlikely to have developed solely through volcanic accumulation processes. The thick syn-extensional volcano-sedimentary successions, reaching 4–5 km in depocenters along the proto-Andean margin (e.g., Cristallini and Ramos, 2000; Heredia et al., 2002), together with widespread caldera-style magmatism, point instead to an overall low-standing landscape shaped by crustal thinning. Under these conditions, the development of a substantial orographic high would have required an additional dynamic support mechanism (cf. Chamberlain et al., 2012). Crucially, our dynamic topography assessment suggests a potential post-subduction uplift of the Choiyoi volcanic edifice of ~0.4–0.7 km, providing a physical basis for the sustained rain shadow and resulting hyperarid conditions inferred inland (Fig. 5). A comparable, case occurred in the western North American Cordillera linked to the Farallon slab removal, where rapid surface uplift (>1 km) during the Eocene coincided with volcanism and extensional tectonics in a non-orogenic setting (Chamberlain et al., 2012).

An alternative explanation for surface uplift during orogenic extension, one not necessarily incompatible with subduction interruption, is lower lithospheric foundering, potentially triggered by substantial crustal thickening (often exceeding 50 km in orogenic plateau settings; e.g., Kay and Kay, 1993). However, geological evidence indicates predominantly shallow marine conditions throughout most of the orogenic evolution along the proto-Andean margin, suggesting such extreme crustal thicknesses were never attained during the Late Carboniferous to earliest Permian (see sections above).

We suggest that reestablished dynamic subsidence after subduction interruption, combined with back-arc extension, thermal subsidence, and elevated global sea levels, contributed to marine inundation beginning in the Late Triassic, becoming widespread by the Early Jurassic (Haq and Cloetingh, 2025; Vicente et al., 2005; Fig. 1b). This transgression, recorded in forearc, proto-Andean, and back-arc regions (Fig. 1c), represents a major reconnection of Panthalassa with southwestern Gondwana (Vicente et al., 2005).

Collectively, stratigraphic, magmatic, and modeled dynamic topography analyses suggest that the protracted disconnection of Panthalassa from the South American margin, and subsequent continentalization of western Gondwana, reflect not only orogenic and magmatic processes but also a deep mantle-driven topographic reorganization (Fig. 5). This finding deepens our understanding of southwestern Gondwana's evolution and emphasizes that subduction dynamics, especially interruptions and slab loss, can leave enduring imprints on Earth's surface.

CRediT authorship contribution statement

Guido M. Gianni: Methodology, Investigation, Formal analysis, Data curation, Conceptualization. **Federico Dávila:** Writing – original draft, Visualization, Validation, Software, Investigation, Formal analysis. **Cesar R. Navarrete:** Visualization, Investigation, Data curation. **Gustavo Correa:** Validation, Investigation, Formal analysis, Data curation. **Osvaldo Conde:** Validation, Investigation, Data curation. **Pietro Sternai:** Validation, Investigation, Formal analysis.

Declaration of competing interest

The authors declare that they have no known competing financial interests or personal relationships that could have appeared to influence the work reported in this paper.

Acknowledgments

G. M. G. was founded by the Alexander von Humboldt Foundation through a research scholarship for experienced researchers. G. M. G. This study is dedicated to P. A. Jaramillo. We are greatly thankful to the reviewers, Dr. Oscar Limarino and Dr. Lijun Liu, for their detailed comments, which substantially improved this study.

Supplementary materials

Supplementary material associated with this article can be found, in the online version, at doi:10.1016/j.epsl.2026.119920.

Data availability

Dynamic topography was computed following the analytical formulation of Hager and O'Connell (1979, 1981), which relates mantle density anomalies to surface deflection through a viscous asthenospheric channel. The original implementation is available through the Geodynamics community notebooks (https://geodynamics.org/resources/notebooks). For this study, the workflow was translated and adapted into a Python environment to facilitate parameter exploration and integration with our regional datasets. The model evaluates the surface response to prescribed lateral variations in mantle density, viscosity, and effective channel thickness over a configurable geographic grid. Outputs consist of gridded dynamic topography fields that are subsequently filtered to emphasize long-wavelength signals relevant to foreland-scale surface deformation. Data and the code can be requested directly to F. Dávila (fmd.geodinamica@gmail.com).

References

Alasino, P.H., Paterson, S.R., Kirsch, M., Larrovere, M.A., 2022. The role of crustal thickness on magma composition in arcs: an example from the pre-Andean, South American Cordillera. Gondwana Res. 106, 191–210.

Archangelsky, S., Cuneo, R., 1987. Feruglioclad aceae, a new conifer family from the permian of Gondwana. Rev. Palaeobot. Palynol. 51, 3–30.

Arvizu, H., Manea, V.C., Oliveros, V., Vásquez, P., 2024. Unraveling the geodynamic evolution of the pre- and early-andean margin: insights from numerical modeling. Geophys. Res. Lett. 51, e2024GL110360.

Bahlburg, H., Vervoort, J.D., Du Frane, S.A., Bock, B., Augustsson, C., Reimann, C., 2009. Timing of crust formation and recycling in accretionary orogens: insights learned from the western margin of South America. Earth-Sci. Rev. 97, 215–241. https://doi.org/10.1016/j.earscirev.2009.01.002.

Balarino, M.L., Correa, G.A., Gutiérrez, P.R., Cariglino, B., Carrevedo, M.L., 2016. The palynology of the La Deheza Formation (Carboniferous–Permian; Upper Palaeozoic), Paganzo Basin, San Juan Province, Argentina. Palynology 40, 172–192.

Balarino, M.L., Correa, G.A., Gutiérrez, P.R., Carrevedo, M.L., 2012. Palinología de la Formación Andapaico (Cisuraliano-Guadalupiano), Precordillera Central Sanjuanina (Argentina): consideraciones bioestratigráficas regionales. Revista Brasileira de Paleontologia.

Bastías-Mercado, F., González, J., Oliveros, V., 2020. Volumetric and compositional estimation of the Choiyoi magmatic province and its comparison with other silicic large igneous provinces. J. South. Am. Earth. Sci. 103, 102749.

Bastos, L.P.H., Rodrigues, R., Pereira, E., Bergamaschi, S., Alferes, C.L.F., Augland, L.E., Domeier, M., Planke, S., Svensen, H.H., 2021. The birth and demise of the vast epicontinental permian Irati-Whitehill sea: evidence from organic geochemistry, geochronology, and paleogeography. Palaeogeogr. Palaeoclim. Palaeoecol. 562, 110103.

Bernardez, S.C.S., Limarino, C.O., Marenssi, S.A., Ciccioli, P.L., 2023. Short note. A new U-Pb age for the Talampaya Formation: stratigraphic and paleoclimatic implications. J. South. Am. Earth. Sci. 128, 104492.

Brandl, P.A., Regelous, M., Beier, C., Haase, K.M., 2013. High mantle temperatures following rifting caused by continental insulation. Nat. Geosci. 6, 391–394.

Bucher, J., Varela, A., D'Elia, L., Bilmes, A., López, M., García, M., Franzese, J., 2020. Multiproxy paleosol evidence for a rain shadow effect linked to miocene uplift of the North Patagonian Andes. Bulletin 132, 1603–1614. https://doi.org/10.1130/B35495.1.

Busquets, P., Colombo, F., Heredia, N., Cardó, R., 2008. Gravitational sliding in a foreland basin. Late Paleozoic, Cordillera Frontal, Andes, San Juan-Argentina. Geo-Temas 10, 466. –466.

Busquets, P., Colombo, F., Heredia, N., de Porta, N.S., Fernandez, L.R., Marrón, J.Á., 2005. Age and tectonostratigraphic significance of the upper carboniferous series in the basement of the Andean Frontal Cordillera: geodynamic implications. Tectonophysics 399, 181–194.

Busquets, P., Limarino, C.O., Cardó, R., Méndez-Bedia, I., Gallastegui, G., Colombo, F., Heredia, N., Césari, S.N., 2013. El neopaleozoico de la Sierra de Castaño (Cordillera Frontal Andina, San Juan, Argentina): reconstrucción tectónica y paleoambiental. Andean Geol. 40, 172–195.

Cane, M.A., Molnar, P., 2001. Closing of the Indonesian seaway as a precursor to East African aridification around 3–4 million years ago. Nature 411, 157–162.

Césari, S.N., Gaido, M.F., Cegarra, M.I., Anselmi, G., et al., 2014. The first record of Permian flora in the Ansilta Formation (western Precordillera of Argentina) and its regional correlation. Ameghiniana 51, 428–432.

Césari, S.N., Limarino, C.O., Gulbranson, E.L., 2011. An upper paleozoic bio-chronostratigraphic scheme for the western margin of Gondwana. Earth-Sci. Rev. 106, 149–160.

Césari, S.N., Limarino, C.O., Marenssi, S., Ciccioli, P.L., Bello, F.C., Ferreira, L.C., Scarlatta, L.R., Friedman, R., 2022. High-precision U-Pb CA-ID-TIMS calibration of the Permian Lueckisporites-dominated assemblages in westernmost Gondwana: inferences for correlations. Palynology 46, 1–20.

Chamberlain, C.P., Mix, H.T., Mulch, A., Hren, M.T., Kent-Corson, M.L., Davis, S.J., Horton, T.W., Graham, S.A., 2012. The cenozoic climatic and topographic evolution of the western North American Cordillera. Am. J. Sci. 312, 213–262. https://doi.org/10.2475/ajs.312.3.213.

Charrier, R., Hervé, F., Muñoz-Gómez, M., Fanning, C.M., Moisan, P., Rebolledo, S., del Castillo, M.R., 2024. The early carboniferous age of the Arrayán Formation in the Choapa accretionary complex: implications for its fossil floral content, tectonic setting and evolution of the southwestern Gondwana margin (north-central Chile). J. South. Am. Earth. Sci. 148, 105161.

Colombo, F., Limarino, C.O., Spalletti, L.A., Busquets, P., Cardó, R., Méndez-Bedia, I., Heredia, N., 2014. Late palaeozoic lithostratigraphy of the Andean Precordillera revisited (San Juan Province, Argentina). J. Iber. Geol.

Cristallini, E.O., Ramos, V.A., 2000. Thick-skinned and thin-skinned thrusting in the La Ramada fold and thrust belt: crustal evolution of the high Andes of San Juan, Argentina (32°S). Tectonophysics 317, 205–235.

Davies, J.H., von Blanckenburg, F., 1995. Slab break-off: a model of lithosphere detachment and its test in the magmatism and deformation of collisional orogens. Earth Planet. Sci. Lett. 129, 85–102. https://doi.org/10.1016/0012-821X(94)00356-3.

Díaz-Martínez, E., Mamet, B., Isaacson, P., Grader, G., 2000. Permian marine sedimentation in northern Chile: new paleontological evidence from the Juan de Morales Formation, and regional paleogeographic implications. J. South. Am. Earth. Sci. 13, 511–525.

Dopico, C.I.M., de Luchi, M.G.L., Rapalini, A.E., Fanning, C.M., Antonio, P.Y., 2019. Geochemistry and geochronology of the shallow-level La Esperanza magmatic system (Permian-Triassic), northern Patagonia. J. South. Am. Earth. Sci. 96, 102347. https://doi.org/10.1016/j.jsames.2019.102347.

Garcia-Castellanos, D., Villaseñor, A., 2011. Messinian salinity crisis regulated by competing tectonics and erosion at the Gibraltar arc. Nature 480, 359–363. https://doi.org/10.1038/nature10634.

García-Sansegundo, J., Farias Arquer, P.J., Heredia Carballo, N., Gallastegui Suárez, G., Charrier, R., Rubio Ordóñez, Á., Cuesta Fernández, A., 2014. Structure of the andean palaeozoic basement in the Chilean coast at 31 degrees 30′S: geodynamic evolution of a subduction margin. J. Iber. Geol. 40, 293–308.

Giambiagi, L., Mescua, J., Bechis, F., Martínez, A., Folguera, A., 2011. Pre-Andean deformation of the Precordillera southern sector, southern Central Andes. Geosphere 7, 219–239.

Gianni, G.M., Luján, S.P., 2021. Geodynamic controls on magmatic arc migration and quiescence. Earth-Sci. Rev. 218, 103676.

Gianni, G.M., Navarrete, C.R., 2022. Catastrophic slab loss in southwestern Pangea preserved in the mantle and igneous record. Nat. Commun. 13, 698.

González, J., Oliveros, V., Lucassen, F., Creixell, C., Coloma, F., Velásquez, R., Hernández, L., Vásquez, P., Kasemann, S.A., 2025. The triassic magmatism in southwestern Gondwana: an example of arc batholith construction in a retreating margin. Gondwana Res. 139, 81–103.

Grader, G., Isaacson, P., Díaz-Martínez, E., Pope, M., 2008. Pennsylvanian and Permian sequences in Bolivia: Direct responses to Gondwana glaciation. Geological Society of America special chapters.

Gulbranson, E.L., Ciccioli, P.L., Montañez, I.P., Marenssi, S.A., Limarino, C.O., Schmitz, M., Davydov, V., 2015. Paleoenvironments and age of the Talampaya Formation: the permo-triassic boundary in northwestern Argentina. J. South. Am. Earth. Sci. 63, 310–322.

Gurnis, M., Mitrovica, J.X., Ritsema, J., van Heijst, H.J., 2000. Constraining mantle density structure using geological evidence of surface uplift rates: the case of the African superplume. Geochem. Geophys. Geosyst. 1. https://doi.org/10.1029/2000GC000040.

Gutiérrez, P.R., Zavattieri, A.M., Noetinger, S., 2018. The Lopingian palynological Guttulapollenites Hannonicus–Cladaitina Veteadensis assemblage zone of Argentina, stratigraphical implications for Gondwana. J. South. Am. Earth. Sci. 88, 673–692.

Hager, B.H., O'Connell, R.J., 1979. Kinematic models of large-scale flow in the earth's mantle. J. Geophys. Res.: Solid Earth 84, 1031–1048. https://doi.org/10.1029/JB084iB03p01031.

Haq, B.U., Cloetingh, S., 2025. Tectonics vs eustasy: the oceanic container and its contents. Earth-Sci. Rev., 105166

Heredia, N., Fernández, L.R., Gallastegui, G., Busquets, P., Colombo, F., 2002. Geological setting of the Argentine Frontal Cordillera in the flat-slab segment (30° 00′–31° 30′ S latitude). J. South. Am. Earth. Sci. 15, 79–99.

Heredia, N., Farias Arquer, P.J., García-Sansegundo, J., Giambiagi, L.B., et al., 2012. The basement of the Andean Frontal Cordillera in the Cordón del Plata (Mendoza, Argentina): geodynamic evolution. Andean. Geol.

Hervé, F., Fanning, C.M., Calderón, M., Mpodozis, C., 2014. Early Permian to Late Triassic batholiths of the Chilean Frontal Cordillera (28–31 S): SHRIMP U–Pb zircon ages and Lu–Hf and O isotope systematics. Lithos 184, 436–446.

Hoggard, M.J., White, N., Al-Attar, D., 2016. Global dynamic topography observations reveal limited influence of large-scale mantle flow. Nat. Geosci. 9, 456–463. https://doi.org/10.1038/ngeo2709.

Iannuzzi, R., Vieira, C.E., Guerra-Sommer, M., Díaz-Martínez, E., Grader, G.W., 2004. Permian plants from the Chutani Formation (Titicaca Group, northern Altiplano of Bolivia): II. The morphogenus glossopteris. An. Acad. Bras. Ciênc. 76, 129–138.

Kay, R.W., Kay, S.M., 1993. Delamination and delamination magmatism. Tectonophysics 219 (1–3), 177–189.

Keidel, J., 1925. Sobre el desarrollo paleogeográfico de las grandes unidades geológicas de la Argentina.

Kern, H.P., Lavina, E.L.C., Paim, P.S.G., Girelli, T.J., Lana, C., 2021. Paleogeographic evolution of the southern Paraná Basin during the Late Permian and its relation to the Gondwanides. Sediment. Geol. 415, 105808.

Kleiman, L.E., Japas, M.S., 2009. The Choiyoi volcanic province at 34°S–36°S (San Rafael, Mendoza, Argentina): implications for the late palaeozoic evolution of the southwestern margin of Gondwana. Tectonophysics 473, 283–299.

Limarino, C.O., Alonso-Muruaga, P.J., Ciccioli, P.L., Loinaze, V.S.P., Césari, S.N., 2014. Stratigraphy and palynology of a late paleozoic glacial paleovalley in the Andean Precordillera, Argentina. Palaeogeogr. Palaeoclim. Palaeoecol. 412, 223–240.

Limarino, C.O., Heredia, N., Spalletti, L.A., Busquets, P., Colombo, F., Méndez-Bedia, I., Cardó, R., Césari, S.N., 2023a. Stratigraphy and tectosedimentary evolution of the late paleozoic ancestral Andes between 33° and 25° SL. J. South. Am. Earth. Sci. 121, 104116.

Limarino, C.O., Bernardez, S.C.S., Marenssi, S.A., Ciccioli, P.L., Cesari, S.N., Ferreira, L., 2023b. Formación Puerta de las Angosturas (Pérmico, provincia de Catamarca): definición, edad y significado estratigráfico. Rev. Asoc. Geol. Argent. 80, 382–403.

Limarino, C.O., Spalletti, L.A., 2006. Paleogeography of the upper paleozoic basins of southern South America: an overview. J. South. Am. Earth. Sci. 22, 134–155.

Liu, L., Spasojevic, S., Gurnis, M., 2008. Reconstructing Farallon plate subduction beneath North America back to the Late Cretaceous. Science 322 (5903), 934–938.

Liu, B., Williams, S., Seton, M., Zhao, G., 2024. Mapping paleoelevations along active continental margins with igneous geochemistry: A case study from South America. Gondwana Research 134, 285–297.

López de Luchi, M.G., Dopico, C.I.M., Rapalini, A.E., 2021. The permian to early triassic granitoids of the Nahuel Niyeu-Yaminué area, northern Patagonia: igneous stratigraphy, geochemistry and emplacement conditions. J. South. Am. Earth. Sci. 106, 102894. https://doi.org/10.1016/j.jsames.2021.102894.

López-Gamundí, O.R., Espejo, I.S., Conaghan, P.J., Powell, C.M., Veevers, J.J., 1994. Southern South America, 18. Geological Society of Australia Special Publication, pp. 1–60.

Malone, J.R., Malone, J., Isbell, J.L., Malone, D.H., Craddock, J.P., Pauls, K., 2024. Unmixing detrital zircon U-Pb ages reveals tectonic and climatic depositional influences on the carboniferous Ansilta Formation. Calingasta-Uspallata Basin west. Argent., Geosci. Front. 15, 101807.

Mancuso, A.C., Krapovickas, V., Marsicano, C., Benavente, C., Benedito, D., De La Fuente, M., Ottone, E.G., 2016. Tetrapod tracks taphonomy in eolian facies from the Permian of Argentina. Palaios. 31, 374–388.

Mpodozis, C., Kay, S.M., 1992. Late paleozoic to triassic evolution of the Gondwana margin: evidence from Chilean Frontal Cordilleran batholiths (28°S to 31°S). Geol. Soc. Am. Bull. 104, 999–1014.

Nina, L., Paula-Santos, G., Sial, A., Bark, G., Wanhainen, C., Jiménez, G., Blanco, M., 2020. Anoxic oceanic conditions during the late permian mass extinction-evidence from the Chutani Formation, Bolivia. J. South. Am. Earth. Sci. 103, 102693.

Oliveros, V., Vásquez, P., Creixell, C., Lucassen, F., Ducea, M.N., Ciocca, I., González, J., Espinoza, M., Salazar, E., Coloma, F., et al., 2020. Lithospheric evolution of the pre- and early andean convergent margin, Chile. Gondwana Res. 80, 202–227.

Pankhurst, R.J., Rapela, C.W., Fanning, C.M., Márquez, M., 2006. Gondwanide continental collision and the origin of Patagonia. Earth-Sci. Rev. 76, 235–257. https://doi.org/10.1016/j.earscirev.2006.03.001.

Pysklywec, R.N., Mitrovica, J.X., 1998. Mantle flow mechanisms for the large-scale subsidence of continental interiors. Geology 26, 687–690. https://doi.org/10.1130/0091-7613(1998)026<0687:MFMFTL>2.3.CO;2.

Ramos, V.A., Lovecchio, J.P., Naipauer, M., Pángaro, F., 2020. The collision of Patagonia: geological facts and speculative interpretations. Ameghiniana 57, 464–479.

del Rey, Á., Deckart, K., Planavsky, N., Arriagada, C., Martínez, F., 2019. Tectonic evolution of the southwestern margin of Pangea and its global implications: evidence from the mid permian–Triassic magmatism along the Chilean-argentine border. Gondwana Res. 76, 303–321. https://doi.org/10.1016/j.gr.2019.06.006.

Ricard, Y., Fleitout, L., Froidevaux, C., 1984. Geoid heights and lithospheric stresses for a dynamic earth. Ann. Geophys. 2, 267–286. https://doi.org/10.1007/s00015-984-0267-2.

Rocha-Campos, A.C., Basei, M.A., Nutman, A.P., Kleiman, L.E., Varela, R., Llambias, E., Canile, F.M., Da Rosa, O.D.C., 2011. 30 million years of permian volcanism recorded in the Choiyoi Igneous Province (W Argentina) and their source for younger ash fall deposits in the Paraná Basin: SHRIMP U–Pb zircon geochronology evidence. Gondwana Res. 19, 509–523.

Sato, A.M., Llambías, E.J., Basei, M.A., Castro, C.E., 2015. Three stages in the late paleozoic to triassic magmatism of southwestern Gondwana, and the relationships with the volcanogenic events in coeval basins. J. South. Am. Earth. Sci. 63, 48–69.

Sato, A.M., Tickyj, H., Llambías, E.J., Sato, K., 2000. The Las Matras tonalitic–trondhjemitic pluton, central Argentina: grenvillian-age constraints, geochemical characteristics, and regional implications. J. South. Am. Earth. Sci. 13, 587–610. https://doi.org/10.1016/S0895-9811(00)00048-3.

Spalletti, L.A., Limarino, C.O., Colombo, F., 2010. Internal anatomy of an erg sequence from the aeolian-fluvial system of the De La Cuesta Formation (Paganzo Basin, northwestern Argentina). Geol. Acta 8 (4), 431–447.

Strazzere, L., Gregori, D.A., Benedini, L., 2016. Early permian arc-related volcanism and sedimentation at the western margin of Gondwana: insight from the Choiyoi Group lower section. Geosci. Front. 7, 715–731.

Taboada, A.C., 2010. Mississippian–Early permian brachiopods from western Argentina: tools for middle-to high-latitude correlation, paleobiogeographic and paleoclimatic reconstruction. Palaeogeogr. Palaeoclim. Palaeoecol. 298, 152–173.

Vázquez, M.S., Césari, S.N., 2017. The Permian palynological Lueckisporites-Weylandites Biozone in the San Rafael Block and its correlation in western Gondwana. J. South. Am. Earth. Sci. 76, 165–181.

Vicente, J.C., et al., 2005. Dynamic paleogeography of the Jurassic Andean basin: pattern of transgression and localisation of main straits through the magmatic arc. Rev. Asoc. Geol. Argent. 60, 221–250.

Whalen, J.B., Hildebrand, R.S., 2019. Trace element discrimination of arc, slab failure, and A-type granitic rocks. Lithos 348, 105179.

Zhang, Y., Shu, Y., Turner, S., Chen, Z., Zeng, Z., Huang, F., 2024. Deciphering contribution of recycled altered oceanic crust to arc magmas using Ba-Sr-Nd isotopes. J. Geophys. Res.: Solid Earth 129, e2023JB028407. https://doi.org/10.1029/2023JB028407.